



Multi-omics staging of locally advanced rectal cancer predicts treatment response: a pilot study

Ilaria Cicalini^{1,2} · Antonio Maria Chiarelli³ · Piero Chiacchiaretta² · David Perpetuini³ · Consuelo Rosa³ · Domenico Mastrodicasa⁴ · Martina d'Annibale⁵ · Stefano Trebeschi⁶ · Francesco Lorenzo Serafini³ · Giulio Cocco^{3,7} · Marco Narciso⁵ · Antonio Corvino⁸ · Sebastiano Cinalli⁹ · Domenico Genovesi¹⁰ · Paola Lanuti^{1,11} · Silvia Valentinuzzi^{1,12} · Damiana Pieragostino^{1,2} · Davide Brocco¹³ · Regina G. H. Beets-Tan^{14,6} · Nicola Tinari¹¹ · Stefano L. Sensi³ · Liborio Stuppia^{1,15} · Piero Del Boccio^{1,12} · Massimo Caulo^{3,5} · Andrea Delli Pizzi^{2,5}

Received: 2 August 2023 / Accepted: 13 March 2024 / Published online: 27 March 2024
© The Author(s) 2024

Abstract

Treatment response assessment of rectal cancer patients is a critical component of personalized cancer care and it allows to identify suitable candidates for organ-preserving strategies. This pilot study employed a novel multi-omics approach combining MRI-based radiomic features and untargeted metabolomics to infer treatment response at staging. The metabolic signature highlighted how tumor cell viability is predictively down-regulated, while the response to oxidative stress was up-regulated in responder patients, showing significantly reduced oxoproline values at baseline compared to non-responder patients (p -value $< 10^{-4}$). Tumors with a high degree of texture homogeneity, as assessed by radiomics, were more likely to achieve a major pathological response (p -value $< 10^{-3}$). A machine learning classifier was implemented to summarize the multi-omics information and discriminate responders and non-responders. Combining all available radiomic and metabolomic features, the classifier delivered an AUC of 0.864 (± 0.083 , p -value $< 10^{-3}$) with a best-point sensitivity of 90.9% and a specificity of 81.8%. Our results suggest that a multi-omics approach, integrating radiomics and metabolomic data, can enhance the predictive value of standard MRI and could help to avoid unnecessary surgical treatments and their associated long-term complications.

Keywords Rectal cancer · Treatment response · Magnetic resonance imaging · Multi-omics · Radiomics · Metabolomics

Introduction

Colorectal cancer (CRC) represents the third most frequent cancer in the world and the fourth cause of cancer death [1]. Currently, the total mesorectal excision (TME) after neoadjuvant chemo-radiotherapy represents the standard of care for patients with locally advanced rectal cancer (LARC) ($\geq T3$ or $N+$) is the total mesorectal excision (TME) after neoadjuvant chemo-radiotherapy (CRT)². Watchful waiting programs allow patients with complete response following CRT (“responders”) to be closely monitored via imaging and endoscopy, opting for organ-preserving treatment strategies; however, these programs are adopted only in selected institutions [2]. LARC receiving neoadjuvant CRT showed complete response rates ranging from 5 to 44% [3]. Recently, there has been a growing interest in new biomarkers of CRT

response to improve patients’ selection for more intensive therapy or watchful waiting.

The gold standard method for staging rectal cancer and evaluating the response to treatment is magnetic resonance imaging (MRI) [4]. Moreover, MRI plays a crucial role in patient selection and monitoring in the watchful waiting strategy [5]. Indeed, MRI demonstrates remarkable precision in qualitatively evaluating prognostic factors, such as tumor location, extent, the distance from the anal sphincter complex, presence of mesorectal fascia infiltration and extramural vascular invasion [6]. In a recent multi-reader study comparing four MRI methods for rectal tumor response evaluation, the average accuracy ranged between 62 and 68% and improved when diffusion-weighted imaging (DWI) was included [7].

Recently, multi-omics approaches investigating CRC at molecular level have shown potential to improve diagnosis and prognostic assessment of colon cancer [8, 9]. Among

Extended author information available on the last page of the article

these “omics” disciplines, “radiomics” and “metabolomics” recently showed the potential predictive role in tumor response assessment [10–13]. The term “radiomics” refers to the application of information engineering approaches to radiologic images delivering a large number of image features related to the shape, intensity and texture heterogeneity within a given volume of interest, otherwise invisible to the naked eye. Tumors are heterogeneous at the genetic and histopathological level, and high intratumoral heterogeneity is associated with a poor prognosis [14]. This approach can overcome the limit of random sampling or biopsy that does not allow for a complete assessment of the phenotype or genetic heterogeneity within a tumor [14]. Based on these characteristics and thanks to the continuous technological improvement, the radiomics approach has been used for the preoperative assessment of treatment response [15–18]. Metabolomics, by studying and quantifying the metabolites present in biological fluids, offers an instant view of the system, providing useful information for understanding the processes taking place in the analyzed organism. Tumor growth follows a variety of metabolic pathways resulting in the accumulation of specific intermediate metabolites and metabolomics represent a growing discipline in the characterization of serum metabolites in cancer [19, 20] can be used as prognostic markers for response to CRT. [21–25]. To date, integrating “-omics” disciplines may represent a new framework for personalized cancer care.

This study presents a cutting-edge multi-omics approach combining MRI-based radiomics features with untargeted metabolomics data, with the aim of developing an experimental workflow capable of predicting the treatment response in patients diagnosed with LARC. This novel non-invasive method called “radiometabolomics” may pave the way to further larger studies improving the role of “omics” disciplines in rectal cancer.

Methods

Subjects

This retrospective study was approved by the local Ethical Committee. A total of 140 consecutive patients who underwent rectal MRI for tumor staging between February 2013 and February 2019 were included (Fig. 1). Inclusion criteria were (1) biopsy-confirmed non-mucinous LARC, (2) 3.0 T MRI examination, (3) clinical outcome assessment on surgical specimen (complete or not complete response), (4) long-course CRT and (5) availability of metabolomics data. In total, 105 patients were excluded: 12 were mucinous cancers, 33 were treated in other centers, and the final clinical outcome was not available, 18 were considered unfit for long-course CRT due to poor clinical conditions stat, 5

patients had severe MR susceptibility artifacts in the pelvis (hip replacement), and 37 had no metabolomics data. The study population was composed of 35 patients. Descriptive baseline characteristics of included patients are detailed in Table 1. The study workflow is shown in Fig. 5.

Chemo-radiotherapy

Long-course radiotherapy consisted of 3D conformal technique. A total dose of 4500 cGy (180 cGy/day) was delivered to the pelvic nodes. It was followed by a sequential boost of 540 cGy (180 cGy/day; total dose 5040 cGy) or a concomitant boost of 1000 cGy (100 cGy/day, 2 times/week; total dose 5500 cGy). It was firstly used a 3D-CRT technique and then a simultaneous integrated boost with intensity-modulated radiotherapy (220 cGy/day, total dose 5500 cGy). 5-Fluorouracil and leucovorin or capecitabine were administered in different schedules as concomitant chemotherapy.

MRI protocol

A 3 T MRI (Achieva, Philips Medical System, Best, the Netherlands) equipped with a phased array surface coil was used for the rectal study. The MRI protocol included T2w and DWI images acquired with a plane perpendicular to the tumor major axis. ADC maps were calculated for each patient. Detailed information about the MRI protocol has been previously documented and is accessible in the supplementary material (Appendix 1) [6, 15, 26].

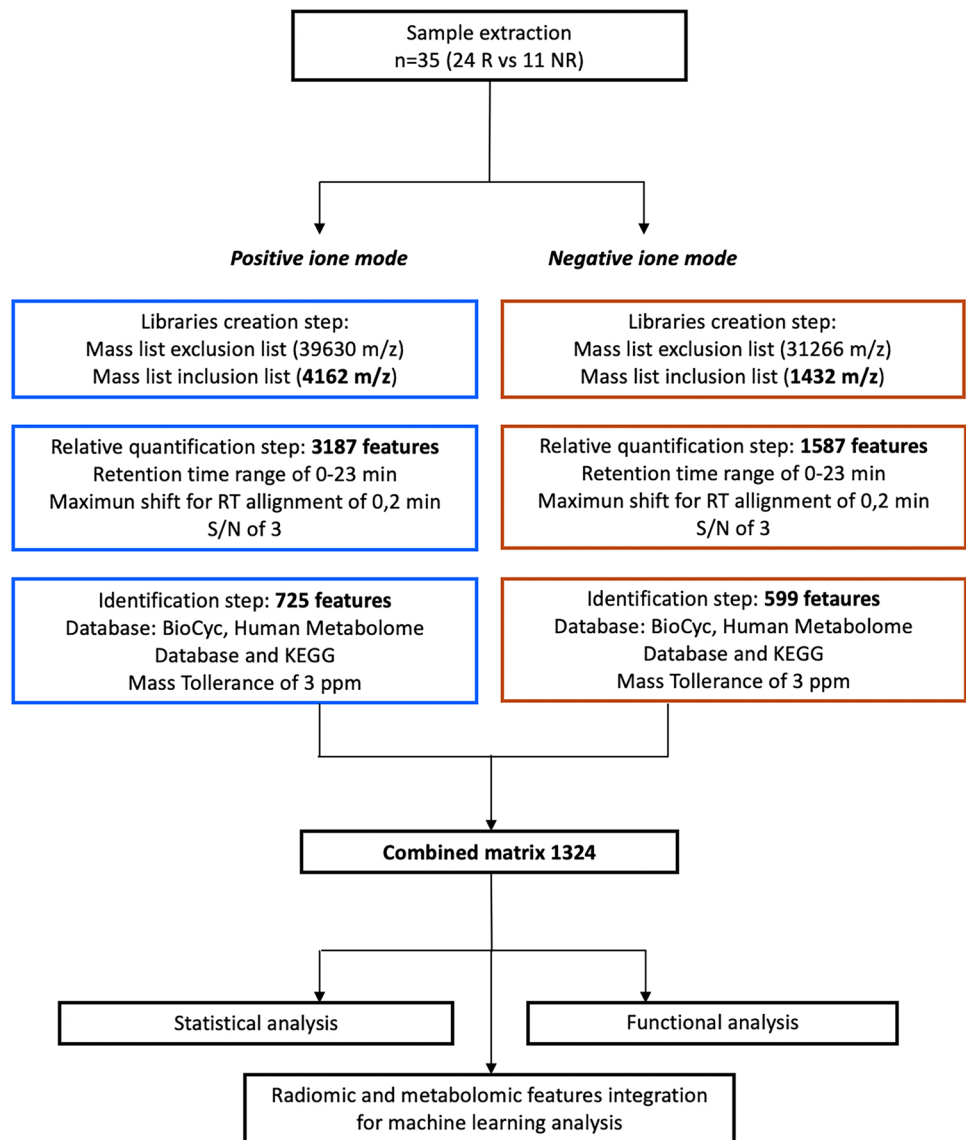
Imaging analysis

Two independent whole-volume tumor segmentations for each patient were manually performed by two readers on T2w and ADC. One reader was a board-certified radiologist with 5 years of expertise in rectal MRI and the other was a senior radiology resident. The tumor presence was defined as intermediate signal intensity on T2w images and a corresponding hypointensity on ADC [4]. All the segmentations were used as masks for the following analysis. An open-source computing platform, 3DSlicer Version 4.8 (www.3dslicer.org), was used for image segmentation [15, 27].

Staging MRI features

Four weeks after the manual segmentation, the two readers evaluated in consensus eight staging MRI-based features (sMRI) on the T2w images. These features regarded tumor location, craniocaudal extension, distance from the internal anal sphincter, mesorectal fascia infiltration, extramural vascular invasion, extramural depth of tumor invasion, T-stage and N-stage [15].

Fig. 1 Workflow of untargeted metabolomics approach. The number of features taken into consideration in the various steps, up to the final data matrix, is shown in bold. Each processing step was described detailing the inclusion and exclusion criteria. Exclusion list includes compounds present in the blank sample that are considered potential contaminants. Inclusion list includes molecules present in the sample excluding contaminants. Chromatographic retention times (RT) and the minimum signal-to-noise ratio (*S/N*) were the inclusion criteria for the quantification step. The databases and the mass tolerance (expressed in ppm) were the inclusion criteria in the identification step



Radiomic features

An open-source platform, PyRadiomics, guided the extraction of radiomics features from the segmentations of the two readers [28]. A reproducibility assessment was performed. Both the MR images and the segmentations were resampled using isotropic voxel dimensions of $1 \times 1 \times 1$ mm to avoid data heterogeneity bias and to ensure reproducibility. Ten built-in filters (original, wavelet, Laplacian of Gaussian (LoG), square, square root, logarithm, exponential, gradient, LBP2D and LBP3D) were utilized to process the data, resulting in the calculation of seven feature classes (first-order statistics, shape descriptors, glcm, glrlm, ngtdm, glcm and glsm).

Blood sample extraction and processing

60 μ L of serum was extracted with 180 μ L of methanol on ice, after 30 min of incubation on ice, the sample was centrifugated at +4 $^{\circ}$ C for 30 min, the supernatant was dried in speedvac and the dry residue was resuspended in 120 μ L by using a mixture of water and acetonitrile (ACN) 30:70 for metabolic analyzes.

Untargeted metabolomics analysis

Ten μ L of extracted metabolites was analyzed in triplicate by LC–MS/MS with a Dionex UltiMate 3000 RSLCnano System (Thermo Fisher Scientific) coupled to an Orbitrap

Table 1 Descriptive baseline characteristics of included patients ($n = 35$)

Variable	Value
Gender	
Male	22 (63%)
Female	13 (37%)
Median age (IQR*)	66 (63–74)
MRI examination	35
Staging MRI Features	
Location	
High	2 (6%)
Middle	17 (48%)
Low	16 (46%)
Craniocaudal Extension, mm (Mean \pm SD)	47 \pm 20
Distance from IAS, mm (Mean \pm SD)	31 \pm 26
Depth of Extramural Invasion, mm (Mean \pm SD)	7 \pm 7
Mesorectal Fascia Infiltration	11 (31%)
Extramural Vascular Invasion	21 (60%)
Primary cT stage**	
T1–T2	2 (6%)
T3	30 (86%)
T4	3 (8%)
Primary cN stage**	
N0	7 (20%)
N1	18 (51%)
N2	10 (29%)
Treatment response***	
Responders	24 (69%)
16 TRG1 (46%)	
8 TRG2 (23%)	
Non-responders	11 (31%)
8 TRG3 (23%)	
3 TRG4 (8%)	

* = IQR Inter-quartile range; SD standard deviation; IAS internal anal sphincter; EMVI extramural vascular invasion

** Assessed with MRI and derived from clinical MRI reports in the hospital's patient database

*** Assessed according to Mandard Tumor Regression Grade (TRG) system on surgical specimen after neoadjuvant treatment

Fusion Tribrid mass spectrometer (Thermo Fisher Scientific), using the Deep Scan AcquireX data dependent acquisition tool. Metabolites were separated on an Accucore™ C18 (2.1 mm I.D., 150 mm L., 2.6 μ m ps, Thermo Fisher Scientific) HPLC column. The flow rate was set to 300 μ L/min with a total run time of 30 min and the following chromatographic gradient (mobile phase A: 0.1% formic acid (FA) in water (H₂O); mobile phase B: 0.1% FA in ACN: from 5 to 70% of B in 13.5 min followed by 70 to 98% in 2 min, maintaining 98% B for 7 min, from 98 to 5% B in 0.5 min and maintaining 5% B until the end of the run). The

mass spectrometer, providing a 60,000 resolution in full scan mode throughout the mass range, was equipped with a H-ESI spray source. The acquisition was achieved in both positive and negative ion polarity, using stepped HCD fragmentation (collision energies: 20, 40 and 120%) and Orbitrap for MS², fixed collision-induced dissociation (CID) fragmentation (collision energy: 35%) and ion trap for MS³. Precursor ions in the range 160 to 2000 m/z with an absolute intensity above 5.0×10^2 were selected for MS², while fragment ions above the threshold of 8.0×10^3 were chosen for MS³. Deep Scan AcquireX data dependent acquisition tool was used by analyzing a representative pool sample for the creation of excluded and included mass list in both MS scan acquisition mode and MS² and MS³ for the identification step.

Metabolomics feature extraction

Raw data were processed using ChemSpider and mzCloud to search databases of MS¹ and fragmentation scans, respectively, in Compound Discoverer version 3.1 (Thermo Fisher Scientific). Mass lists of “Endogenous Metabolites Database 4400 Compounds” and “Extractables and Leachables HRAM Compound Database” were used as well, mostly to recognize contaminants. Metabolite identification was based on accurate mass and mass fragmentation pattern spectra, but annotation required at least in part a manual contribution after applying the FISH scoring. A mass tolerance of 3 ppm was set for feature matching, and the log₂ fold change was used to compare the differential abundance of compounds in each sample.

Functional analysis of metabolomics signature

Metabolites ratios were uploaded for “Core Analysis” through Ingenuity Pathway Analysis (IPA software, Qiagen, Hilden, Germany) to statistically map the modulated molecules for their functional annotations in terms of canonical pathways, upstream regulators analysis and downstream effects networks. Molecular pathways and predicted upstream regulators with overlap p -value < 0.05 and activation z -score > 2 or < -2 were considered as meaningful on both statistical and biological points of view.

Machine learning: kNN-based classification

Machine learning (ML) approaches aim to exploit data multi-dimensionality to identify statistical dependences among variables for predictive, modeling and classification purposes. In this study, the k -nearest neighbors (kNN) classifier was employed to classify the responder and non-responder groups [29]. The kNN classifier labels a new instance based on the majority class of the k closest instances from the training data. The kNN algorithm commences by

receiving an instance whose class label is unknown. Using a distance metric, such as Euclidean distance, it then computes the distance between this new instance and every instance in the training set. Next, it selects the k instances from the training set that are closest to the new instance based on their distance from the new instance. The new instance is then tagged with the class label that is most prevalent among its k -nearest neighbors (“majority vote”). k is a user-specified parameter that can be selected by cross-validation or other methods. Larger values of k result in a smoother decision boundary, while smaller values of k result in a more complex decision boundary. One of the benefits of k NN is that it is simple and easy to understand. However, it can be computationally expensive, particularly when the size of the training set size is large [13]. sMRI features, radiomic features (ADC and T2w evaluated by two operators) and metabolomic data (MD) were considered as input of the machinery, both independently and together, thus allowing to develop five different models relying on, respectively, sMRI only, MD only, ADC only, T2w only and sMRI + MD + ADC + T2w. The classifier’s input data were normalized (z-score), whereas the output was defined labeling the non-responder patients as class “0” and the responder participants as class “1.” The Euclidean distance was employed as the distance metric, the weights assigned to the k -nearest neighbors were the inverse of the squared distance, and the number of neighbors was considered as an hyperparameter of the model and it was optimized within the nested cross-validation framework [30–32].

To mitigate the poor generalization performances potentially deriving from the large number of features with respect to samples, feature selection procedures were employed [33]. Feature selection was performed in two steps. Firstly, a subset of the available features was selected considering only those features with a high “inter-observer” reliability, i.e., only those robust to differences introduced by the manual identification of the region of interest by the independent radiologists. Radiomics features with high inter-observer correlation ($r > 0.95$) were considered reliable and used for further analysis [34, 35]. Of note, such feature selection was performed outside the nested cross-validation. In fact, this feature selection does not exploit data output label and does not create classification overfitting. The second step of feature selection was performed implementing a wrapper method [36, 37]. In this study, a sequential forward selection was employed: It started with no feature in the model, and in each iteration, a feature was added to produce the highest increase in performance until the addition of a new variable did not improve the model’s performance. Differently to the first step of feature selection, the wrapper method exploits the output labels and creates data overfitting without samples separation in train and test sets. Hence, similarly to the hyperparameter optimization of the k NN classifiers,

the wrapper approach was iterated within the nested cross-validation (nCV).

To optimize hyperparameters and ensure the model’s generalizability without overfitting, three distinct datasets are necessary. Firstly, a training set is used to train the model with various hyperparameter values. Secondly, a validation set is employed to select the best hyperparameters based on performance. Finally, a test set is used to evaluate the final model’s performance. This approach allows for effective hyperparameter tuning and unbiased assessment of the model’s performance on unseen data. However, when a reduced sample numerosity is available, this data separation might drastically reduce the training sample, making it difficult for the data-driven model to be properly fitted. The nCV is an extension of this method that helps to reduce the impact of sample loss across multiple sets while avoiding results biases and data overfitting [30–32]. In detail, data are separated into folds, and the model is trained iteratively in a nested way on all but onefold of the data. The inner loop identifies the optimal hyperparameters (validation, in our case it identified also features employing the wrapper method) while the outer loop estimates how well the model performs over iterations (test). The approach is described as leave-one-out nCV if the number of folds equals the number of samples (onefold per sample) [38, 39]. This method is ideal for medical settings because each sample corresponds to a single patient. In this study, a leave-one-out nCV was used to train, validate and test the k NN model. To define the optimal model hyperparameter and identify the selected features reported in the manuscript, a majority voting algorithm was employed across the cross-validation iterations. Since the study sample provided non-balanced classes, an iterative procedure (1000 iterations) was performed to train and test the machinery with balanced classes via random subsampling of the larger class at each iteration. The ML analysis was implemented in MATLAB (MATLAB 2021b©, Mathworks Natick, MA, USA).

Reference standard

For all patients, a Tumor Regression Grade (TRG) 1 or 2, assessed according to Mandard’s classification, was considered as major pathological response [40–42].

In detail, TRG1 and TRG2 were labeled as responders (R) while TRG3 and TRG4 as non-responders (NR) [43].

Statistical analysis

The classification performance was assessed by evaluating the confusion matrix associated with the out-of-training samples, which provides information about the sensitivity and specificity of the classifier. In addition, the receiver operating characteristic (ROC) analysis was employed,

considering the area under the ROC curve (AUC) as indicative of the classification performance of each proposed model. Since a bootstrap procedure was implemented to balance the classes randomly, the average AUC and the standard deviation of the distribution delivered by the procedure are reported. The p -values associated with the average AUCs (probability of obtaining an AUC value above 0.5 by chance) and that associated with average AUCs comparisons (probability of two AUCs being generated from the same underlying distribution) were evaluated generating a metrics' confidence interval through a bootstrapping approach (1000 iterations). The statistical analysis was performed in MATLAB (MATLAB 2021b©, Mathworks Natick, MA, USA). PLS-DA and volcano plot for metabolomics data were performed by the online tool Metaboanalyst (<https://www.metaboanalyst.ca/>). Violin plot were performed with BoxPlotR online tool, and correlation and Heatmaps were performed with GraphPad Prism 7.

Results

Staging MRI features

Nine MRI staging features (sMRI) were evaluated by radiologists (refer to the method section for further information). Of the nine features, the only feature that was different on average between the 24 responders (R) and 11 non-responders (NR) was the mesorectal fascia infiltration ($p < 0.05$).

Radiomics

In total, 1470 features were extracted with PyRadiomics for each subject, image type and reader. Of these 1470 features, 919 for apparent diffusion coefficient (ADC) and 916 for T2-weighted (T2w) images were highly reproducible ($r > 0.95$) when computed within the masks identified by the two radiologists. The reproducible features were averaged between the two readers and were used for further analysis. Of the selected features, 109 for the ADC and 124 for the T2w images showed significant average differences between the 24 R and 11 NR ($p < 0.05$, uncorrected).

Metabolomics

Sera from 24 R and 11 NR were analyzed using an untargeted metabolomics approach, to identify and relatively quantify as many serum metabolites as possible. Following the workflow shown in Fig. 1, a representative pool of blood samples was used to build a library of mass spectra and fragmentation mass spectra for the metabolite identification step, in both positive and negative acquisition mode. In this phase of library construction, the triplicate analysis

of a blank sample allowed us to create a mass exclusion list composed of 39,630 m/z and 31,266 m/z for acquisition in positive and negative mode, respectively. At the same time, the analysis of a representative sample allowed us to create an inclusion list of species to be quantified and identified in the next step on the samples individually (4162 and 1432 species in positive and negative mode, respectively), as summarized in the workflow in Fig. 1. In the following step, samples from 35 patients were individually analyzed in mass scanning in both positive and negative acquisition mode, to obtain a chromatographic profile for the metabolite's relative quantification step. In total, 3187 and 1587 features were quantified in positive and negative modes, based on the following quantification parameters: Retention time (RT) 0–23 min, maximum shift for allign RT = 0.2 min and signal-to-noise ratio $S/N = 3$.

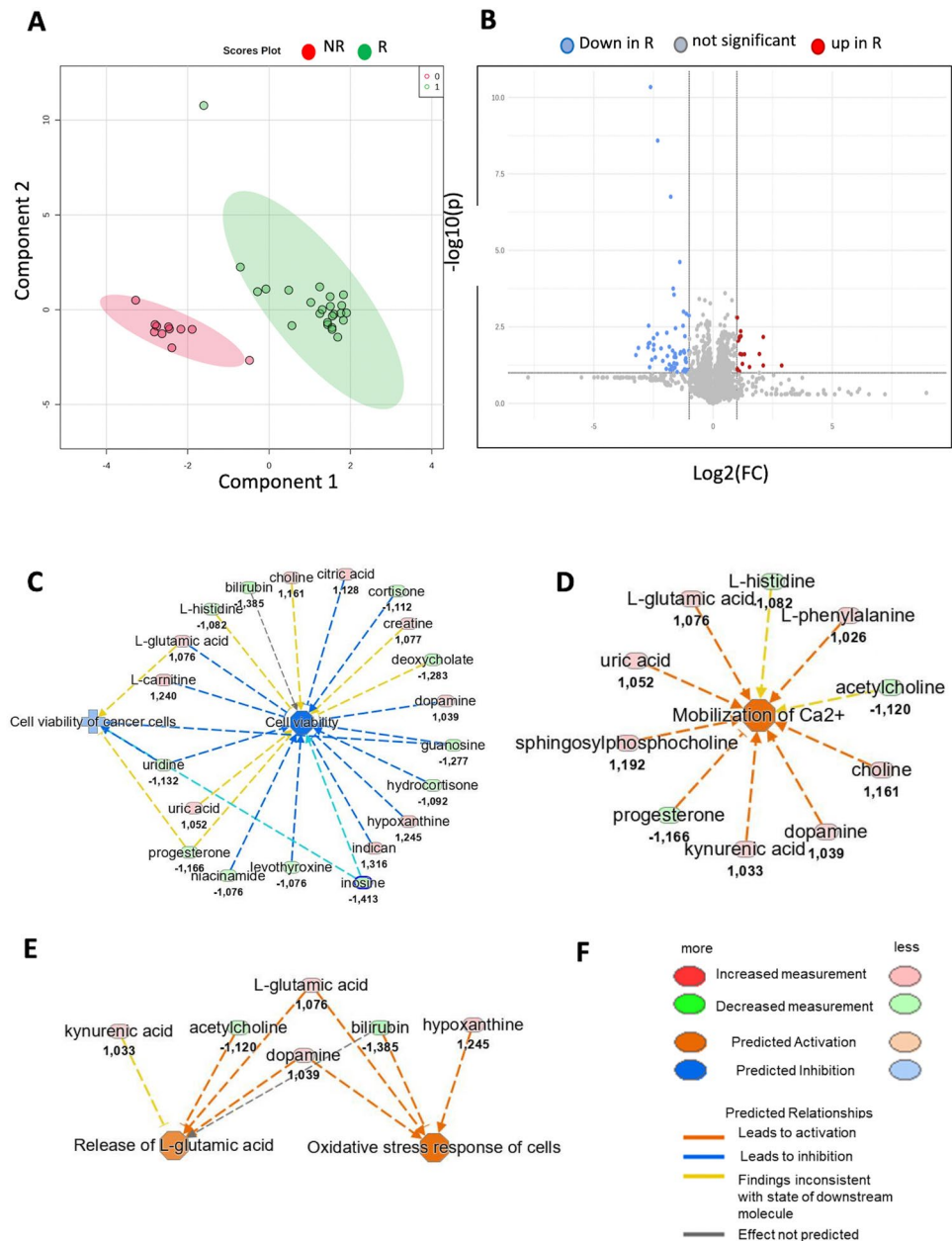
Of these, 1,324 features were identified as specific metabolites by matching with the library of the acquired fragmentation mass spectra. The databases used for identification were BioCyc, Human Metabolome Database and KEGG, considering a mass tolerance of 3 ppm.

The identified metabolites were used for statistical analysis and functional analysis through the Ingenuity Pathway Analysis (IPA software, Qiagen, Hilden, Germany) bioinformatics tool and machine learning analysis. The sparse partial least-squares discriminant analysis (sPLS-DA) algorithm was applied as exploratory multivariate statistical analysis (Fig. 2A), indicating that metabolomics serum signatures could distinguish R from NR patients at T0. Univariate statistical analysis revealed 75 compounds significantly different when comparing R and NR at T0, as shown in the volcano plot in Fig. 2B. IPA functional investigation of the endogenous compounds identified, quantified and mapped in the Kyoto Encyclopedia of Genes and Genomes (KEGG) and Human Metabolome Database (HMDB), highlighted a predicted down-regulation of “Cell viability” and “Cell viability of cancer cells” (p -value = $2.09 \text{ E}10^{-3}$; z -score = -1.86) biological function in R patients compared to NR patients, before CRT (Fig. 2C). Moreover, in R patients, IPA investigation highlighted a predicted significant up-regulation of the following cellular functions: “Mobilization of Ca^{2+} ” (p -value = $1.74 \text{ E}10^{-5}$; z -score = $+2.17$), “Oxidative stress response of cells” (p -value = $2.97 \text{ E}10^{-4}$; z -score = $+1.98$) and “Release of L-glutamic acid” (p -value = $6.15 \text{ E}10^{-5}$; z -score = $+1.17$) (Fig. 2D–E).

Multi-omics kNN-based classification

When using the k-Nearest Neighbors (kNN) classifier on sMRI metrics, only the Mesorectal Fascia Infiltration was selected via the wrapper procedure. The classification performance evaluation delivered an out-of-training sample ROC with an AUC of 0.636 (± 0.094 , p -value = 0.10). The

Fig. 2 **A** sPLS-DA based on 4000 features in the plasma of responder (R) and non-responder (NR) patients. **B** Volcano plot of 4000 metabolomic features classifying them in not significant (gray), significantly down-regulated in RP (blue dots) and significantly up-regulated in RP (red dots). **C** Prediction of down-regulated cellular functions “Cell viability” and “Cell viability of cancer cells” in R patients. **D** Predicted of up-regulated cellular function “Mobilization of Ca²⁺” in R patients. **E** Predicted up-regulation of cellular function “Oxidative stress response of cells” and “Release of l-glutamic acid” in R patients. **F** Legend of color code for increased and decreased measurement of metabolites, and predicted activation and inhibition of disease and cellular function



optimized cutoff point delivered an out-of-training sample sensitivity of 54.5% and an out-of-training sample specificity of 72.7%. In Fig. 3A, ROC curve is presented together with the associated confusion matrix for the optimized cutoff point.

When using metrics extracted from apparent diffusion coefficient (ADC) maps, the “original_shape_Maximum2D-DiameterSlice” and “wavelet_LLH_glrIm_RunLengthNon-Uniformity” features were selected. The machine learning (ML) framework achieved ROC performance with an AUC of 0.807 (± 0.097 , p -value = 0.001) and a best sensitivity of 90.9% coupled with a specificity of 72.7% (Fig. 3B).

As concerns the T2w analysis, 4 features were selected: exponential_firstorder_Energy, “squareroot_glm_Inverse-Variance,” “wavelet_LLH_glszm_SizeZoneNonUniformity” and “lbp_3D_m1_glrIm_RunLengthNonUniformity.” An AUC of 0.826 (± 0.097 , p -value = 0.0007) coupled with a best-point sensitivity and a specificity of 82.6% were obtained (Fig. 3C).

Feature selection on metabolomic data (MD) identified 2 salient compounds, oxoproline and proline. The classification delivered an AUC = 0.809 (± 0.041 , p -value = 0.001) with best sensitivity of 90.9% and specificity of 72.7% (Fig. 3D).

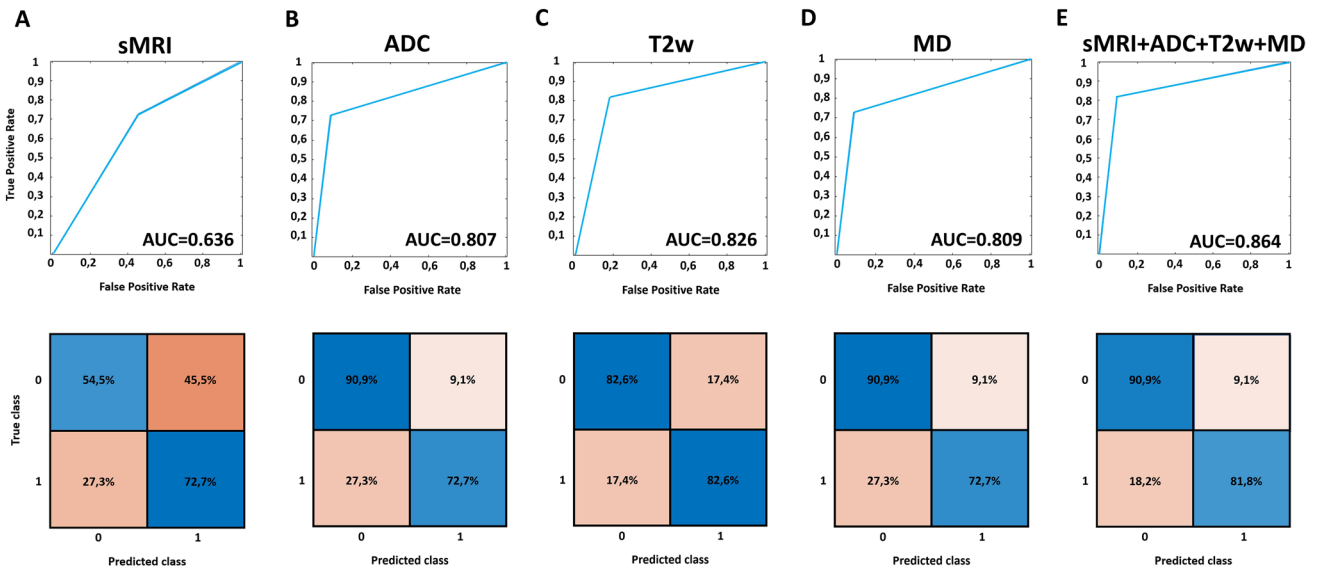


Fig. 3 ROC curve and best cutoff point confusion matrix delivered by the classification performed relying on **A** sMRI data, **B** ADC metrics, **C** T2w metrics, **D** MD data and **E** sMRI + ADC + T2w + MD data

Table 2 Classification performances of the proposed models expressed as AUC, sensitivity and specificity

Technique	AUC	Sensitivity (%)	Specificity (%)	Selected features
sMRI	0.636	54.5	72.7	Mesorectal Fascia Infiltration
MD	0.809	90.9	72.7	Oxoproline Proline
ADC	0.807	90.9	72.7	original_shape_Maximum2DDiameterSlice wavelet_LLH_glrIm_RunLengthNonUniformity
T2w	0.826	82.6	82.6	exponential_firstorder_Energy squareroot_glcM_InverseVariance wavelet_HHL_glszm_SizeZoneNonUniformity lbp_3D_m1_glrIm_RunLengthNonUniformity
MD + ADC + T2w	0.864	90.9	81.8	ADC: wavelet_LLH_glrIm_RunLengthNonUniformity gradient_glszm_GrayLevelNonUniformity T2w: wavelet_HHH_glcM_DifferenceAverage MD: Oxoproline

When considering all the available features (i.e., sMRI + ADC + T2w + MD), 4 features were identified as the most predictive by the wrapper procedure: “wavelet_LLH_glrIm_RunLengthNonUniformity” and “gradient_glszm_GrayLevelNonUniformity” from ADC images, “wavelet_HHH_glcM_DifferenceAverage” from T2w images and oxoproline from MD data. The AUC obtained was 0.864 (± 0.083 , p -value = 0.0002) with a best-point sensitivity of 90.9% and a specificity of 81.8% (Fig. 3E). The performances of the investigated models are reported in Table 2. Notably, when comparing the AUC of the different models, statistically significant differences were found when comparing sMRI-based classification with the multi-omics classification (Tables 3 and 4).

Table 3 Comparison between the AUCs of the developed models

Comparisons	z-stat	p-value
MD vs. ADC	0.019	0.985
MD vs. T2w	-0.101	0.867
ADC vs. T2w	-0.187	0.851
MD + ADC + T2w vs. MD	0.577	0.564
MD + ADC + T2w vs. ADC	0.596	0.551
MD + ADC + T2w vs. T2w	0.410	0.682
sMRI vs. MD	-1.411	0.158
sMRI vs. ADC	-1.392	0.164
sMRI vs. T2w	-1.573	0.115
sMRI vs. MD + ADC + T2w	-1.970	0.048

Table 4 Statistical test (Chi-square stat and t-stat) between the two groups (non-responders vs. responders) for the metrics identified by the feature selection procedures

	Metric	Chi-square stat	<i>p</i> -value
sMRI	mesorectal fascia infiltration	3.978	0.046
	Metric	t-stat	<i>p</i> -value
MD	Proline	− 1.173	0.249
	4-Oxoproline	4.910	2.40×10^{-5}
ADC	original_shape_Maximum2DDiameterSlice	3.386	0.002
	wavelet_LLH_glrlm_RunLengthNonUniformity	3.704	7.73×10^{-4}
	squareroot_glszm_LargeAreaLowGrayLevelEmphasis	− 0.689	0.495
	wavelet_HHL_firstorder_Energy	2.695	0.011
T2w	exponential_firstorder_Energy	2.155	0.039
	squareroot_glcM_InverseVariance	2.345	0.025
	wavelet_HHL_glszm_SizeZoneNonUniformity	0.725	0.473
	lbp_3D_m1_glrlm_RunLengthNonUniformity	4.208	1.85×10^{-4}
	wavelet_HHH_glcM_DifferenceAverage	− 0.879	0.385

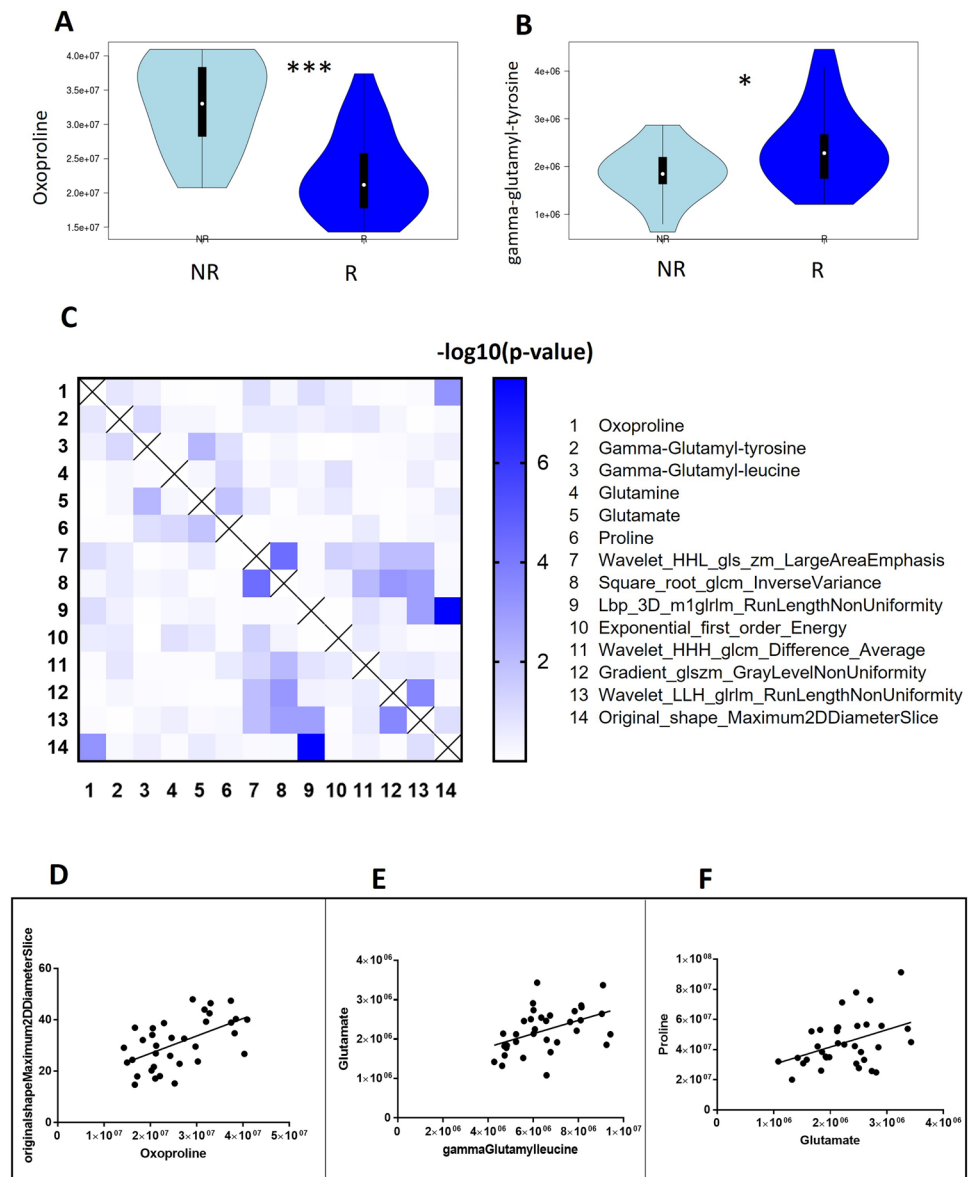
Inferential description of the selected features

Oxoproline levels were significantly (p -value = 0.0001) higher in NR patients (Fig. 4A). Interestingly, oxoproline is considered an oxidative stress marker, involved in the synthesis and degradation of glutathione in the glutathione cycle [44]. In this context, in addition to oxoproline, the gamma-glutamyl amino acids, glutamate, glutamine and proline are also involved. Thus, we extrapolated some of these identified and quantified molecules from the metabolomics data. Among all, gamma-glutamyl-tyrosine levels were significantly higher (p -value = 0.04) in responding patients before starting CRT (Fig. 4B). Furthermore, to integrate the data obtained from metabolomics and radiomics, we created a correlation matrix between the metabolites involved in the degradation and synthesis of glutathione's cycle (numbers 1 to 6 of Fig. 4C legend) along with the main radiomics features (numbers 7–14 of Fig. 4C legend). Pearson correlation coefficients (r) were transformed into $-\log_{10}(p\text{-value})$ and plotted as a Heatmap (Fig. 4C). R -coefficients and p -values calculated for each correlation are provided in Appendix 2 and 3 (Supplementary Material). As shown in the heatmap, significant correlations were found between the same metabolites and radiomics features. A significant moderate correlation was found between oxoproline levels and radiomics features “original shape maximum 2D diameter slice” with $r = 0.557$ and p -value = 0.0006 (Fig. 4D). Moreover, a significant fair correlation was observed between gamma-glutamyl-leucine and glutamate levels ($r = 0.453$ and p -value = 0.007), and between glutamate and proline levels ($r = 0.405$ and p -value = 0.001), as shown in Fig. 4 Panels E–F, respectively (Fig. 5).

Discussion

Our study provided initial evidence that an MRI-based “radiometabolomic” approach has the potential to accurately predict treatment response of patients with LARC with high accuracy and at an early stage. This innovative approach, based on the integration of two -omics methods, could be transferred to the clinic in future, thus improving the patient selection for the most appropriate treatment. More in detail, adding radiometabolomics features to standard T2w conventional clinical features significantly improved the prognostic model. This work confirmed the preliminary results of recent radiomics studies on rectal cancer. Delli Pizzi et al. recently reported that a pre-treatment MRI-based radiomics ML model accurately predicts the treatment response in patients with LARC [15]. Similarly, Shin et al. presented a T2w and ADC-based radiomics model showing better classification performance than radiologists for diagnosing complete response after the completion of CRT [45]. Wang et al. reported that a radiomics model using pre-treatment radiotherapy planning CT images can predict treatment response and survival outcomes in LARC patients [46]. In our study, the predictive radiomics features were extracted from 1 mm slice thickness. In this regard, the last European Society of Gastrointestinal and Abdominal Imaging (ESGAR) consensus recommended that the slice thickness of the axial T2w image should be equal or inferior to 3 mm [4]. The predictive features of our study were mainly focused on tumor heterogeneity. For instance, tumors with a high degree of texture homogeneity were more likely associated with good treatment response. This result is in line with several previous non-rectal cancer studies showing that

Fig. 4 **A, B** Violin plot showing the distribution of oxoproline (Panel A) and gamma-glutamyl-tyrosine (Panel B) for non-responder (in red) and responder (in green) patients. **C** Heatmap of the p -value for the correlation of 14 radiometabolomics features described in the legend on the right. **D** Pearson correlation between oxoproline levels and radiomics features called (original shape maximum 2D diameter slice). **E** Pearson correlation between gamma-glutamyl-leucine and glutamate levels. **F** Pearson correlation between glutamate and proline level. *** means p -value of Mann–Whitney test < 0.001 , * means p -value of Mann–Whitney test < 0.05



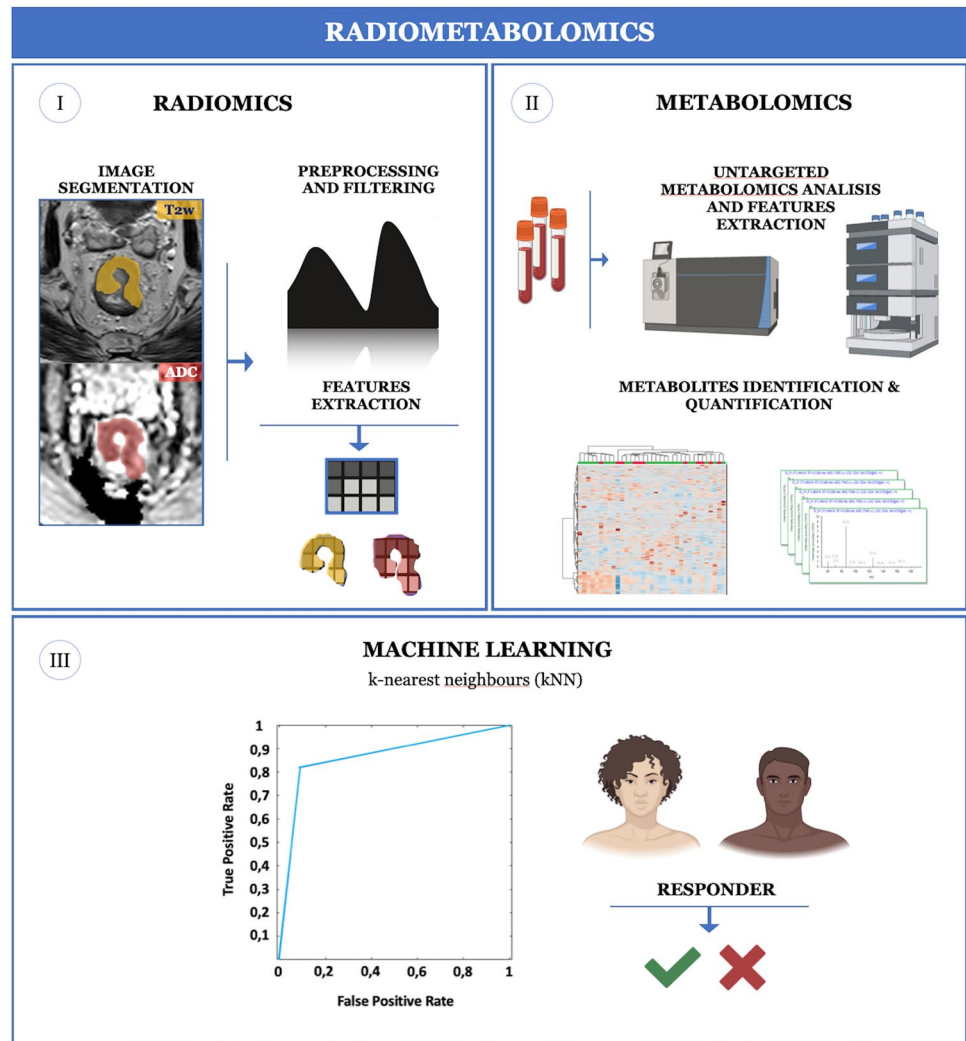
homogeneous texture features are associated with better clinical prognosis and neoadjuvant CRT response [14, 47, 48].

Our results suggested that treatment response prediction improves when imaging-based radiomics is combined with metabolomics. Metabolomics is an emerging field dedicated to the study of metabolites, their composition, interactions, dynamics and responses to diseases or therapies in cells, tissues and biofluids. The application of untargeted metabolomic analysis on peripheral blood may provide novel biomarkers of cancer treatment response [49]. Recently, Yang et al. investigated postoperative esophageal tissue via an untargeted metabolomics approach hypothesizing glycerophospholipids metabolism as a potential therapeutic target of tumor progression [50]. Moreover, several studies have recently explored metabolomics approaches in different

fields of oncology, such as triple-negative breast cancer, gastric cancer and lung cancer [51–53]. For CRC, Brezmes et al. explored urinary NMR-based metabolomics to find novel biomarkers [54]. In addition, metabolic profile investigation associated with gut microbiome composition was recently applied to investigate potential diagnostic markers of individuals with CRC compared to healthy controls [55].

In our study, serum metabolic signature before treatment is significantly correlated to a down-regulation of the vitality of cancer cells in R compared to NR, highlighting how the metabolic study of serum before starting therapy can provide valuable information on outcome. Contextually, the expression of specific serum metabolites in R has highlighted a significant implication in oxidative stress response. Oxoproline accumulation coupled with low levels of gamma-glutamyl-tyrosine in NR patients may suggest a dysregulation

Fig. 5 Study workflow. In the first step (I), rectal cancer was manually segmented on MR images (T2w, ADC), followed by radiomics features extraction. In the second step (II), plasma untargeted metabolomics analysis and metabolites identification and quantification were performed. In the final step (III), a machine learning algorithm (k-nearest neighbors—kNN) was used to select radiometabolomics features and ROC analysis delivered the classification model accuracy for treatment response prediction (created with BioRender.com)



in glutathione degradation and therefore a worse response to oxidative stress [56]. In our study, oxoprolin levels were correlated with the tumor's maximum diameter of the tumor measured on axial MR images (Fig. 4C).

This is, to our knowledge, the first study investigating the potential synergistic role of radiomics and metabolomics in rectal cancer, a translational research field we named “radiometabolomics.” A multi-disciplinary approach involving radiologists, oncologists, biochemists, radiation therapists and bioinformatics may support clinicians in selecting the most appropriate treatment tailored for each patient. This study aims to point out a proof-of-concept experimental workflow combining multi-omics features to explore new possible and pioneer strategies that, once overcome some limitations, could be ready to be moved into clinical practices. Firstly, the sample size is limited and obtained through a single-center retrospective study. Of note, in our work the implementation of the leave-one-out nCV minimized the effect of the reduced number of samples while avoiding overfitting [30]. It was

also coupled with a robust feature selection approach (wrapper method), hence obtaining the maximum classification performance achievable with the available data no bias and good generalization. Because of the absence of analysis bias, an increase in the training sample size is expected to only improve the classification performance. Nonetheless, future studies, possibly prospective and multicenter, are needed to corroborate our findings and to obtain standardized multivariate models that can be routinely used in the clinical practice. Secondly, our 3 T MR scanner was scheduled over time and during the study for software upgrades which might have modified image quality. However, these changes did not cause changes in main MRI protocol parameters. Thirdly, we only used T2w imaging and DWI, without considering dynamic contrast-enhanced imaging (DCE). Nonetheless, the role of DCE in the primary staging of rectal cancer is controversial. In fact, according to the recent ESGAR consensus meeting, the use of DCE-MRI is not routinely recommended [4].

Conclusion

Multi-omics staging has the potential to predict CRT response in patients with LARC, thus enhancing the predictive value of standard MRI and helping to avoid unnecessary surgical treatment. The proposed radiometabolomics integrated approach is into an embryonic phase which may encourage and promote deeper investigation in larger, prospective studies to push toward a better definition of the radiometabolomics role in personalized rectal cancer care.

Supplementary Information The online version contains supplementary material available at <https://doi.org/10.1007/s11547-024-01811-0>.

Acknowledgements The authors thank Daniele Petrucci and Darien Calvo Garcia for their insightful contribution to the MRI protocol settings and imaging data acquisition.

Author contributions ADP conceived and developed the research idea with the assistance of DG, PDB, IC, DPi, PL, SLS, LS and RBT. The study was designed by ADP, MC, CR and ST. Md'A and ADP performed the segmentation task. IC, PDB, DPi and SV designed the metabolomics study. FLS, GC, MN, SC, NT, DB and AC collected the data. IC and SV acquired the metabolomics data, and the processing was supervised by PDB, PC and DP. PCh, DPe, PC and AMC performed the computational experiments with guidance from ADP. ADP, IC and DM wrote the original draft. All authors contributed to paper editing and reviewing, and they have read and approved the final version submitted.

Funding Open access funding provided by Università degli Studi G. D'Annunzio Chieti Pescara within the CRUI-CARE Agreement. The authors have not disclosed any funding.

Data availability The datasets generated during and/or analyzed during the current study are not publicly available due to the clinical and confidential nature of the material. However, they can be made available from the corresponding author on reasonable request.

Declarations

Conflict of interest The authors declare they have no competing interests.

Ethical approval This study received formal approval (protocol ID “richhh5td,” approved on 22/07/2020) from the Ethical Committee of the University G. d'Annunzio of Chieti-Pescara, Italy; informed consent was waived by the same ethics committee that approved the study (Comitato Etico per la Ricerca Biomedica delle Province di Chieti e Pescara e dell'Università degli Studi “G. d'Annunzio” di Chieti e Pescara). The study was conducted according to ethical principles laid down by the latest version of the Declaration of Helsinki.

Open Access This article is licensed under a Creative Commons Attribution 4.0 International License, which permits use, sharing, adaptation, distribution and reproduction in any medium or format, as long as you give appropriate credit to the original author(s) and the source, provide a link to the Creative Commons licence, and indicate if changes were made. The images or other third party material in this article are included in the article's Creative Commons licence, unless indicated otherwise in a credit line to the material. If material is not included in the article's Creative Commons licence and your intended use is not

permitted by statutory regulation or exceeds the permitted use, you will need to obtain permission directly from the copyright holder. To view a copy of this licence, visit <http://creativecommons.org/licenses/by/4.0/>.

References

1. Araghi M, Soerjomataram I, Jenkins M, Brierley J, Morris E, Bray F, Arnold M (2019) Global trends in colorectal cancer mortality: projections to the year 2035. *Int J Cancer* 144(12):2992–3000. <https://doi.org/10.1002/ijc.32055>
2. Habr-Gama A, Perez RO, Nadalin W, Sabbaga J, Ribeiro U Jr, Silva e Sousa AH Jr, Campos FG, Kiss DR, Gama-Rodrigues J (2004) Operative versus nonoperative treatment for stage 0 distal rectal cancer following chemoradiation therapy: long-term results. *Ann Surg* 240(4):711–717. <https://doi.org/10.1097/01.sla.0000141194.27992.32>. (discussion 717–718)
3. van der Valk MJM, Hilling DE, Bastiaannet E, Meershoek-Klein Kranenbarg E, Beets GL, Figueiredo NL, Habr-Gama A, Perez RO, Renehan AG, van de Velde CJH, Consortium I (2018) Long-term outcomes of clinical complete responders after neoadjuvant treatment for rectal cancer in the International Watch & Wait Database (IWW): an international multicentre registry study. *Lancet* 391(10139):2537–2545. [https://doi.org/10.1016/S0140-6736\(18\)31078-X](https://doi.org/10.1016/S0140-6736(18)31078-X)
4. Beets-Tan RGH, Lambregts DMJ, Maas M, Bipat S, Barbaro B, Curvo-Semedo L, Fenlon HM, Gollub MJ, Gourtsoyianni S, Halligan S, Hoeffel C, Kim SH, Laghi A, Maier A, Rafaelsen SR, Stoker J, Taylor SA, Torkzad MR, Blomqvist L (2018) Magnetic resonance imaging for clinical management of rectal cancer: updated recommendations from the 2016 European Society of Gastrointestinal and Abdominal Radiology (ESGAR) consensus meeting. *Eur Radiol* 28(4):1465–1475. <https://doi.org/10.1007/s00330-017-5026-2>
5. Jayaprakasam VS, Alvarez J, Omer DM, Gollub MJ, Smith JJ, Petkovska I (2023) Watch-and-wait approach to rectal cancer: the role of imaging. *Radiology*. <https://doi.org/10.1148/radiol.221529>
6. Delli Pizzi A, Basilico R, Cianci R, Seccia B, Timpani M, Tavoleta A, Caposiena D, Faricelli B, Gabrielli D, Caulo M (2018) Rectal cancer MRI: protocols, signs and future perspectives radiologists should consider in everyday clinical practice. *Insights Imaging* 9(4):405–412. <https://doi.org/10.1007/s13244-018-0606-5>
7. El Khababi N, Beets-Tan RGH, Tissier R, Lahaye MJ, Maas M, Curvo-Semedo L, Dresen RC, Nougaret S, Beets GL, Lambregts DMJ (2022) Comparison of MRI response evaluation methods in rectal cancer: a multicentre and multireader validation study. *Eur Radiol*. <https://doi.org/10.1007/s00330-022-09342-w>
8. Diez-Villanueva A, Sanz-Pamplona R, Sole X, Cordero D, Crous-Bou M, Guino E, Lopez-Doriga A, Berenguer A, Ausso S, Pare-Brunet L, Obon-Santacana M, Moratalla-Navarro F, Salazar R, Sanjuan X, Santos C, Biondo S, Diez-Obrero V, Garcia-Serrano A, Alonso MH, Carreras-Torres R, Closa A, Moreno V (2022) COLONOMICS—integrative omics data of one hundred paired normal-tumoral samples from colon cancer patients. *Sci Data* 9(1):595. <https://doi.org/10.1038/s41597-022-01697-5>
9. Fernandez-Rozadilla C, Timofeeva M, Chen Z, Law P, Thomas M, Schmit S, Diez-Obrero V, Hsu L, Fernandez-Tajes J, Palles C, Sherwood K, Briggs S, Svinti V, Donnelly K, Farrington S, Blackmur J, Vaughan-Shaw P, Shu XO, Long J, Cai Q, Guo X, Lu Y, Broderick P, Studd J, Huyghe J, Harrison T, Conti D, Dampier C, Devall M, Schumacher F, Melas M, Rennert G, Obon-Santacana M, Martin-Sanchez V, Moratalla-Navarro F, Oh JH, Kim J, Jee


- SH, Jung KJ, Kweon SS, Shin MH, Shin A, Ahn YO, Kim DH, Oze I, Wen W, Matsuo K, Matsuda K, Tanikawa C, Ren Z, Gao YT, Jia WH, Hopper J, Jenkins M, Win AK, Pai R, Figueiredo J, Haile R, Gallinger S, Woods M, Newcomb P, Duggan D, Cheadle J, Kaplan R, Maughan T, Kerr R, Kerr D, Kirac I, Bohm J, Mecklin LP, Jousilahti P, Knekt P, Aaltonen L, Rissanen H, Pukkala E, Eriksson J, Cajuso T, Hanninen U, Kondelin J, Palin K, Tanskanen T, Renkonen-Sinisalo L, Zanke B, Mannisto S, Albanes D, Weinstein S, Ruiz-Narvaez E, Palmer J, Buchanan D, Platz E, Visvanathan K, Ulrich C, Siegel E, Brezina S, Gsur A, Campbell P, Chang-Claude J, Hoffmeister M, Brenner H, Slattery M, Potter J, Tsilidis K, Schulze M, Gunter M, Murphy N, Castells A, Castellvi-Bel S, Moreira L, Arndt V, Shcherbina A, Stern M, Pardamean B, Bishop T, Giles G, Southey M, Idos G, McDonnell K, Abu-Ful Z, Greenon J, Shulman K, Lejbkowitz F, Offit K, Su YR, Steinfeld R, Keku T, van Guelpen B, Hudson T, Hampel H, Pearlman R, Berndt S, Hayes R, Martinez ME, Thomas S, Corley D, Pharoah P, Larsson S, Yen Y, Lenz HJ, White E, Li L, Doheny K, Pugh E, Shelford T, Chan A, Cruz-Correa M, Lindblom A, Hunter D, Joshi A, Schafmayer C, Scacheri P, Kundaje A, Nickerson D, Schoen R, Hampe J, Stadler Z, Vodicka P, Vodickova L, Vymetalkova V, Papadopoulos N, Edlund C, Gauderman W, Thomas D, Shibata D, Toland A, Markowitz S, Kim A, Chanock S, van Duijnhoven F, Feskens E, Sakoda L, Gago-Dominguez M, Wolk A, Naccarati A, Pardini B, FitzGerald L, Lee SC, Ogino S, Bien S, Kooperberg C, Li C, Lin Y, Prentice R, Qu C, Bezieau S, Tangen C, Mardis E, Yamaji T, Sawada N, Iwasaki M, Haiman C, Le Marchand L, Wu A, Qu C, McNeil C, Coetzee G, Hayward C, Deary I, Harris S, Theodoratou E, Reid S, Walker M, Ooi LY, Moreno V, Casey G, Gruber S, Tomlinson I, Zheng W, Dunlop M, Houlston R, Peters U (2023) Deciphering colorectal cancer genetics through multi-omic analysis of 100,204 cases and 154,587 controls of European and east Asian ancestries. *Nat Genet* 55(1):89–99. <https://doi.org/10.1038/s41588-022-01222-9>
10. Gillies RJ, Kinahan PE, Hricak H (2016) Radiomics: images are more than pictures, they are data. *Radiology* 278(2):563–577. <https://doi.org/10.1148/radiol.2015151169>
 11. Kaushik AK, De Berardinis RJ (2018) Applications of metabolomics to study cancer metabolism. *Bba-Rev Cancer* 1870(1):2–14. <https://doi.org/10.1016/j.bbcan.2018.04.009>
 12. Pieragostino D, Agnifili L, Fasanella V, D'Aguanno S, Mastropasqua R, Di Ilio C, Sacchetta P, Urbani A, Del Boccio P (2013) Shotgun proteomics reveals specific modulated protein patterns in tears of patients with primary open angle glaucoma naive to therapy. *Mol Biosyst* 9(6):1108–1116. <https://doi.org/10.1039/c3mb25463a>
 13. Kramer O (2013) K-Nearest Neighbors. In: Dimensionality reduction with unsupervised nearest neighbors. *Intelligent Systems Reference Library*. pp 13–23. doi:https://doi.org/10.1007/978-3-642-38652-7_2
 14. Davnall F, Yip CS, Ljungqvist G, Selmi M, Ng F, Sanghera B, Ganeshan B, Miles KA, Cook GJ, Goh V (2012) Assessment of tumor heterogeneity: an emerging imaging tool for clinical practice? *Insights Imaging* 3(6):573–589. <https://doi.org/10.1007/s13244-012-0196-6>
 15. Delli Pizzi A, Chiarelli AM, Chiacchiaretta P, d'Annibale M, Croce P, Rosa C, Mastrodicasa D, Trebeschi S, Lambregts DMJ, Caposiena D, Serafini FL, Basilico R, Cocco G, Di Sebastiano P, Cinalli S, Ferretti A, Wise RG, Genovesi D, Beets-Tan RGH, Caulo M (2021) MRI-based clinical-radiomics model predicts tumor response before treatment in locally advanced rectal cancer. *Sci Rep* 11(1):5379. <https://doi.org/10.1038/s41598-021-84816-3>
 16. Horvat N, Veerarraghavan H, Khan M, Blazic I, Zheng J, Capanu M, Sala E, Garcia-Aguilar J, Gollub MJ, Petkovska I (2018) MR imaging of rectal cancer: radiomics analysis to assess treatment response after neoadjuvant therapy. *Radiology* 287(3):833–843. <https://doi.org/10.1148/radiol.2018172300>
 17. Li C, Yin J (2021) Radiomics based on T2-weighted imaging and apparent diffusion coefficient images for preoperative evaluation of lymph node metastasis in rectal cancer patients. *Front Oncol* 11:671354. <https://doi.org/10.3389/fonc.2021.671354>
 18. Ma X, Shen F, Jia Y, Xia Y, Li Q, Lu J (2019) MRI-based radiomics of rectal cancer: preoperative assessment of the pathological features. *BMC Med Imaging* 19(1):86. <https://doi.org/10.1186/s12880-019-0392-7>
 19. Brown DG, Rao S, Weir TL, O'Malia J, Bazan M, Brown RJ, Ryan EP (2016) Metabolomics and metabolic pathway networks from human colorectal cancers, adjacent mucosa, and stool. *Cancer Metab* 4:11. <https://doi.org/10.1186/s40170-016-0151-y>
 20. Yachida S, Mizutani S, Shiroma H, Shiba S, Nakajima T, Sakamoto T, Watanabe H, Masuda K, Nishimoto Y, Kubo M, Hosoda F, Rokutan H, Matsumoto M, Takamaru H, Yamada M, Matsuda T, Iwasaki M, Yamaji T, Yachida T, Soga T, Kurokawa K, Toyoda A, Ogura Y, Hayashi T, Hatakeyama M, Nakagama H, Saito Y, Fukuda S, Shibata T, Yamada T (2019) Metagenomic and metabolomic analyses reveal distinct stage-specific phenotypes of the gut microbiota in colorectal cancer. *Nat Med* 25(6):968–976. <https://doi.org/10.1038/s41591-019-0458-7>
 21. Chauvin A, Boisvert FM (2018) Clinical proteomics in colorectal cancer, a promising tool for improving personalised medicine. *Proteomes*. <https://doi.org/10.3390/proteomes6040049>
 22. Del Boccio P, Perrotti F, Rossi C, Cicalini I, Di Santo S, Zucchelli M, Sacchetta P, Genovesi D, Pieragostino D (2017) Serum lipidomic study reveals potential early biomarkers for predicting response to chemoradiation therapy in advanced rectal cancer: a pilot study. *Adv Radiat Oncol* 2(2):118–124. <https://doi.org/10.1016/j.adro.2016.12.005>
 23. Fernandes Messias MC, Mecatti GC, Figueiredo Angolini CF, Eberlin MN, Credidio L, Real Martinez CA, Rodrigues Coy CS, de Oliveira CP (2017) Plasma lipidomic signature of rectal adenocarcinoma reveals potential biomarkers. *Front Oncol* 7:325. <https://doi.org/10.3389/fonc.2017.00325>
 24. Patterson NH, Alabdulkarim B, Lazaris A, Thomas A, Marcinkiewicz MM, Gao ZH, Vermeulen PB, Chaurand P, Metrakos P (2016) Assessment of pathological response to therapy using lipid mass spectrometry imaging. *Sci Rep* 6:36814. <https://doi.org/10.1038/srep36814>
 25. Wang H, Ji D, Tian H, Gao Z, Song C, Jia J, Cui X, Zhong L, Shen J, Gu J (2022) Predictive value of proteomic markers for advanced rectal cancer with neoadjuvant chemoradiotherapy. *BMC Cancer* 22(1):868. <https://doi.org/10.1186/s12885-022-09960-z>
 26. Delli Pizzi A, Caposiena D, Mastrodicasa D, Trebeschi S, Lambregts D, Rosa C, Cianci R, Seccia B, Sessa B, Di Flaminio FM, Chiacchiaretta P, Caravatta L, Cinalli S, Di Sebastiano P, Caulo M, Genovesi D, Beets-Tan R, Basilico R (2019) Tumor detectability and conspicuity comparison of standard b1000 and ultrahigh b2000 diffusion-weighted imaging in rectal cancer. *Abdom Radiol (NY)* 44(11):3595–3605. <https://doi.org/10.1007/s00261-019-02177-y>
 27. Cox RW (1996) AFNI: software for analysis and visualization of functional magnetic resonance neuroimages. *Comput Biomed Res* 29(3):162–173. <https://doi.org/10.1006/cbmr.1996.0014>
 28. van Griethuysen JJM, Fedorov A, Parmar C, Hosny A, Aucoin N, Narayan V, Beets-Tan RGH, Fillion-Robin JC, Pieper S, Aerts H (2017) Computational radiomics system to decode the radiographic phenotype. *Cancer Res* 77(21):e104–e107. <https://doi.org/10.1158/0008-5472.CAN-17-0339>
 29. Abu Alfeilat HA, Hassanat ABA, Lasassmeh O, Tarawneh AS, Alhasanat MB, Eyal Salman HS, Prasath VBS (2019) Effects of distance measure choice on K-nearest neighbor classifier

- performance: a review. *Big Data* 7(4):221–248. <https://doi.org/10.1089/big.2018.0175>
30. Filzmoser P, Liebmann B, Varmuza K (2009) Repeated double cross validation. *J Chemom* 23(4):160–171. <https://doi.org/10.1002/cem.1225>
 31. Krstajic D, Buturovic LJ, Leahy DE, Thomas S (2014) Cross-validation pitfalls when selecting and assessing regression and classification models. *J Cheminf* 6(1):10. <https://doi.org/10.1186/1758-2946-6-10>
 32. Liu R, Gillies DF (2016) Overfitting in linear feature extraction for classification of high-dimensional image data. *Pattern Recogn* 53:73–86. <https://doi.org/10.1016/j.patcog.2015.11.015>
 33. Traverso A, Wee L, Dekker A, Gillies R (2018) repeatability and reproducibility of radiomic features: a systematic review. *Int J Radiat Oncol Biol Phys* 102(4):1143–1158. <https://doi.org/10.1016/j.ijrobp.2018.05.053>
 34. Delli Pizzi A, Chiarelli AM, Chiacchiaretta P, d'Annibale M, Croce P, Rosa C, Mastrodicasa D, Trebeschi S, Lambregts DMJ, Caposiena D, Serafini FL, Basilico R, Cocco G, Di Sebastiano P, Cinalli S, Ferretti A, Wise RG, Genovesi D, Beets-Tan RGH, Caulo M (2021) MRI-based clinical-radiomics model predicts tumor response before treatment in locally advanced rectal cancer. *Sci Rep*. <https://doi.org/10.1038/s41598-021-84816-3>
 35. Delli Pizzi A, Chiarelli AM, Chiacchiaretta P, Valdesi C, Croce P, Mastrodicasa D, Villani M, Trebeschi S, Serafini FL, Rosa C, Cocco G, Luberti R, Conte S, Mazzamurro L, Mereu M, Patea RL, Panara V, Marinari S, Vecchiet J, Caulo M (2021) Radiomics-based machine learning differentiates “ground-glass” opacities due to COVID-19 from acute non-COVID-19 lung disease. *Sci Rep*. <https://doi.org/10.1038/s41598-021-96755-0>
 36. Kohavi R, John GH (1997) Wrappers for feature subset selection. *Artif Intell* 97(1–2):273–324. [https://doi.org/10.1016/s0004-3702\(97\)00043-x](https://doi.org/10.1016/s0004-3702(97)00043-x)
 37. Parmar C, Grossmann P, Bussink J, Lambin P, Aerts H (2015) Machine learning methods for quantitative radiomic biomarkers. *Sci Rep* 5:13087. <https://doi.org/10.1038/srep13087>
 38. Kearns M, Ron D (1999) Algorithmic stability and sanity-check bounds for leave-one-out cross-validation. *Neural Comput* 11(6):1427–1453. <https://doi.org/10.1162/089976699300016304>
 39. Perpetuini D, Filippini C, Zito M, Cardone D, Merla A (2022) Altered microcirculation in alzheimer’s disease assessed by machine learning applied to functional thermal imaging data. *Bioengineering (Basel)*. <https://doi.org/10.3390/bioengineering9100492>
 40. Lupattelli M, Matrone F, Gambacorta MA, Osti M, Macchia G, Palazzari E, Nicosia L, Navarria F, Chiloiro G, Valentini V, Aristei C, De Paoli A (2017) Preoperative intensity-modulated radiotherapy with a simultaneous integrated boost combined with Capecitabine in locally advanced rectal cancer: short-term results of a multicentric study. *Radiat Oncol* 12(1):139. <https://doi.org/10.1186/s13014-017-0870-4>
 41. Mandard AM, Dalibard F, Mandard JC, Marnay J, Henry-Amar M, Petiot JF, Roussel A, Jacob JH, Segol P, Samama G et al (1994) Pathologic assessment of tumor regression after preoperative chemoradiotherapy of esophageal carcinoma. *Clinicopathol Correl Cancer* 73(11):2680–2686. [https://doi.org/10.1002/1097-0142\(19940601\)73:11%3c2680::aid-cnrcr2820731105%3e3.0.co;2-c](https://doi.org/10.1002/1097-0142(19940601)73:11%3c2680::aid-cnrcr2820731105%3e3.0.co;2-c)
 42. Valentini V, Gambacorta MA, Cellini F, Aristei C, Coco C, Barbaro B, Alfieri S, D’Ugo D, Persiani R, Deodato F, Crucitti A, Lupattelli M, Mantello G, Navarria F, Belluco C, Buonadonna A, Boso C, Lonardi S, Caravatta L, Barba MC, Vecchio FM, Maranzano E, Genovesi D, Doglietto GB, Morganti AG, La Torre G, Pucciarelli S, De Paoli A (2019) The INTERACT Trial: Long-term results of a randomised trial on preoperative capecitabine-based radiochemotherapy intensified by concomitant boost or oxaliplatin, for cT2 (distal)-cT3 rectal cancer. *Radiother Oncol* 134:110–118. <https://doi.org/10.1016/j.radonc.2018.11.023>
 43. Gonçalves-Ribeiro S, Sanz-Pamplona R, Vidal A, Sanjuan X, Guillen Díaz-Maroto N, Soriano A, Guardiola J, Albert N, Martínez-Villacampa M, López I, Santos C, Serra-Musach J, Salazar R, Capellà G, Villanueva A, Molleví DG (2017) Prediction of pathological response to neoadjuvant treatment in rectal cancer with a two-protein immunohistochemical score derived from stromal gene-profiling. *Ann Oncol* 28(9):2160–2168. <https://doi.org/10.1093/annonc/mdx293>
 44. Bachhawat AK, Yadav S (2018) The glutathione cycle: Glutathione metabolism beyond the gamma-glutamyl cycle. *IUBMB Life* 70(7):585–592. <https://doi.org/10.1002/iub.1756>
 45. Shin J, Seo N, Baek S-E, Son N-H, Lim JS, Kim NK, Koom WS, Kim S (2022) MRI radiomics model predicts pathologic complete response of rectal cancer following chemoradiotherapy. *Radiology* 303(2):351–358. <https://doi.org/10.1148/radiol.211986>
 46. Wang F, Tan BF, Poh SS, Siow TR, Lim FLWT, Yip CSP, Wang MLC, Nei W, Tan HQ (2022) Predicting outcomes for locally advanced rectal cancer treated with neoadjuvant chemoradiation with CT-based radiomics. *Sci Rep*. <https://doi.org/10.1038/s41598-022-10175-2>
 47. Batra SK, Chee CG, Kim YH, Lee KH, Lee YJ, Park JH, Lee HS, Ahn S, Kim B (2017) CT texture analysis in patients with locally advanced rectal cancer treated with neoadjuvant chemoradiotherapy: a potential imaging biomarker for treatment response and prognosis. *Plos One*. <https://doi.org/10.1371/journal.pone.0182883>
 48. Miles KA, Ganeshan B, Griffiths MR, Young RC, Chatwin CR (2009) Colorectal cancer: texture analysis of portal phase hepatic CT images as a potential marker of survival. *Radiology* 250(2):444–452. <https://doi.org/10.1148/radiol.2502071879>
 49. Boroughs LK, DeBerardinis RJ (2015) Metabolic pathways promoting cancer cell survival and growth. *Nat Cell Biol* 17(4):351–359. <https://doi.org/10.1038/ncb3124>
 50. Yang T, Hui R, Nouws J, Sauler M, Zeng T, Wu Q (2022) Untargeted metabolomics analysis of esophageal squamous cell cancer progression. *J Transl Med* 20(1):127. <https://doi.org/10.1186/s12967-022-03311-z>
 51. Wang G, Qiu M, Xing X, Zhou J, Yao H, Li M, Yin R, Hou Y, Li Y, Pan S, Huang Y, Yang F, Bai F, Nie H, Di S, Guo L, Meng Z, Wang J, Yin Y (2022) Lung cancer scRNA-seq and lipidomics reveal aberrant lipid metabolism for early-stage diagnosis. *Sci Transl Med* 14(630):eabk2756. <https://doi.org/10.1126/scitranslmed.abk2756>
 52. Wang J, Kunzke T, Prade VM, Shen J, Buck A, Feuchtinger A, Haffner I, Luber B, Liu DHW, Langer R, Lordick F, Sun N, Walch A (2022) Spatial metabolomics identifies distinct tumor-specific subtypes in gastric cancer patients. *Clin Cancer Res* 28(13):2865–2877. <https://doi.org/10.1158/1078-0432.CCR-21-4383>
 53. Xiao Y, Ma D, Yang YS, Yang F, Ding JH, Gong Y, Jiang L, Ge LP, Wu SY, Yu Q, Zhang Q, Bertucci F, Sun Q, Hu X, Li DQ, Shao ZM, Jiang YZ (2022) Comprehensive metabolomics expands precision medicine for triple-negative breast cancer. *Cell Res* 32(5):477–490. <https://doi.org/10.1038/s41422-022-00614-0>
 54. Brezmes J, Llambrich M, Cumeras R, Guma J (2022) Urine NMR metabolomics for precision oncology in colorectal cancer. *Int J Mol Sci*. <https://doi.org/10.3390/ijms231911171>
 55. Chen F, Dai X, Zhou CC, Li KX, Zhang YJ, Lou XY, Zhu YM, Sun YL, Peng BX, Cui W (2022) Integrated analysis of the faecal metagenome and serum metabolome reveals the role of gut microbiome-associated metabolites in the detection of colorectal cancer and adenoma. *Gut* 71(7):1315–1325. <https://doi.org/10.1136/gutjnl-2020-323476>
 56. Pederzolli CD, Mescka CP, Zandona BR, de Moura CD, Sgaravatti AM, Sgarbi MB, de Souza Wyse AT, Duval Wannmacher CM,

Wajner M, Vargas CR, Dutra-Filho CS (2010) Acute administration of 5-oxoproline induces oxidative damage to lipids and proteins and impairs antioxidant defenses in cerebral cortex and cerebellum of young rats. *Metab Brain Dis* 25(2):145–154. <https://doi.org/10.1007/s11011-010-9190-1>

Publisher's Note Springer Nature remains neutral with regard to jurisdictional claims in published maps and institutional affiliations.

Authors and Affiliations

Ilaria Cicalini^{1,2} · Antonio Maria Chiarelli³ · Piero Chiacchiaretta²  · David Perpetuini³ · Consuelo Rosa³ · Domenico Mastrodicasa⁴ · Martina d'Annibale⁵ · Stefano Trebeschi⁶ · Francesco Lorenzo Serafini³ · Giulio Cocco^{3,7} · Marco Narciso⁵ · Antonio Corvino⁸ · Sebastiano Cinalli⁹ · Domenico Genovesi¹⁰ · Paola Lanuti^{1,11} · Silvia Valentinuzzi^{1,12} · Damiana Pieragostino^{1,2} · Davide Brocco¹³ · Regina G. H. Beets-Tan^{14,6} · Nicola Tinari¹¹ · Stefano L. Sensi³ · Liborio Stuppia^{1,15} · Piero Del Boccio^{1,12} · Massimo Caulo^{3,5} · Andrea Delli Pizzi^{2,5}

✉ Piero Chiacchiaretta
p.chiacchiaretta@unich.it

¹ Center for Advanced Studies and Technology (CAST), University “G. d’Annunzio” of Chieti-Pescara, Chieti, Italy

² Department of Innovative Technologies in Medicine and Odontoiatry, “G. d’Annunzio” University, Chieti, Italy

³ Department of Neuroscience, Imaging and Clinical Sciences, “G. d’Annunzio” University, Chieti, Italy

⁴ Department of Radiology, Stanford University School of Medicine, Stanford, CA, USA

⁵ Department of Radiology, SS. Annunziata Hospital, “G. d’Annunzio” University, Via dei Vestini, 66100 ChietiChieti, Italy

⁶ Department of Radiology, Netherlands Cancer Institute, Amsterdam, The Netherlands

⁷ Unit of Ultrasound in Internal Medicine, Department of Medicine and Science of Aging, “G. D’Annunzio” University, Chieti, Italy

⁸ Medical, Movement and Wellbeing Sciences Department, Via Medina 40, 80133 Naples, Italy

⁹ Division of Pathology, ASST of Valtellina and Alto Lario, Sondrio, Italy

¹⁰ Department of Medical, Oral and Biotechnological Sciences and CeSI-MeT, “G. D’Annunzio” University of Chieti, Via dei Vestini, 66100 Chieti, Italy

¹¹ Department of Medicine and Aging Science, “G. D’Annunzio” University of Chieti, Via dei Vestini, 66100 Chieti, Italy

¹² Department of Pharmacy, “G. D’Annunzio” University of Chieti, Via dei Vestini, 66100 Chieti, Italy

¹³ Clinical Oncology Unit, SS. Annunziata Hospital, Via dei Vestini, 66100 Chieti, Italy

¹⁴ GROW School for Oncology and Developmental Biology, Maastricht University, Maastricht, The Netherlands

¹⁵ Department of Psychological, Health and Territory Sciences, “G. d’Annunzio” University of Chieti-Pescara, 66100 Chieti, Italy